scientific reports

Check for updates

OPEN

Sugarcane bagasse derived biochar potential to improve soil structure and water availability in texturally different soils

Farzad Moradi-Choghamarani[1], Ali Akbar Moosavi[1]✉ & Ali Reza Sepaskhah[2]

Low organic matter content is one of the main constraints in arid and semiarid regions. This constraint and its negative influences on soils and plant growth may be alleviated by biochar (BC). Furthermore, improving soil physical and hydraulic attributes by application of biochar has received increased attention. Therefore, in the present study, the effects of sugarcane bagasse-derived biochar on the structural stability, water availability, and pore-size distribution (PSD) of three texturally different calcareous soils collected from different agro-climatologically regions were examined during a long-term experiment. Low and high-temperature biochars, produced in a muffle furnace by the traditional slow pyrolysis method at 300 °C (BC300) and 600 °C (BC600) were evaluated. Pots (15 kg) were filled with three different silty-clay Inceptisols (SCInc), silty-clay-loam Alfisols (SCLAlf), and loam Aridisols (LArid) soils mixed with 0 (control), 1, 2, and 3 w/w% of BC300 and BC600 during 540 days of incubation. The high energy moisture characteristic (HEMC) data was modeled using a modified van Genuchten function to quantify aggregate stability through stability ratio (SR) and structural stability index (SSI). The plant available water (PAW), least limiting water range (LLWR), and integral water capacity (IWC) were calculated with two matric suctions (h) of 330 cm for field capacity (FC) and 15,000 cm for permanent wilting point (PWP). Then the integral energy (EI) values were calculated (EI_{IWC}). Results indicated that the incorporation of 3 w/w% biochar significantly ($p < 0.01$) increased SR (35 to 100%) and SSI (21 to 28%) indices in all three soils. Biochar significantly increased modal suction (MS) in LArid soils (5 to 158%); whereas, decreased MS of the other soils (3 to 43%). MS, SR, and SSI of BC300 and BC600-treated soils were not significantly different. PAW, LLWR, and IWC significantly decreased in the SCInc (18 to 61%, 8 to 44%, and 6 to 35%) and SCLAlf (8 to 44%, 18 to 35%, and 20 to 47%) soils and increased in LArid (4 to 54%, 3 to 61%, and 24 to 111%) soil with increasing biochar doses. There were no changes in EI_{IWC} in biochar-treated LArid soil where PAW, LLWR, and IWC increased. Biochar increased EI_{IWC} across the studied soil from 1% to 3.38 folds, thereby increasing the gradient of water potential to absorb the available water. Soil and soil-biochar mixtures exhibited heterogeneous and multimodal pore-size distribution (PSD). Biochar promoted the PSD peaks related to water-transmitting pores in SCInc and SCLAlf soils while decreased in LArid soil. In conclusion, results indicated that among the applied levels of biochar, the application of 3 w/w% biochar is suggested as a suitable way to improve soil physical behavior and structural stability.

Keywords High energy moisture characteristic, Integral water capacity, Least limiting water range, Plant available water, Pore-size distribution, Multimodal water retention, Structural stability index

Abbreviations

SCInc	Silty-clay Inceptisol (–)
SCLAlf	Silty-clay-loam Alfisol (–)
LArid	Loam Aridisol (–)
BC300	Sugarcane bagasse-derived biochar produced at 300 °C (–)
BC600	Sugarcane bagasse-derived biochar produced at 600 °C

[1]Department of Soil Science, College of Agriculture, Shiraz University, Shiraz, Iran. [2]Department of Water Engineering, College of Agriculture, Shiraz University, Shiraz, Iran. ✉email: aamousavi@gmail.com; aamousavi@shirazu.ac.ir

GSD	Grain size distribution (–)
P	Mean annual precipitation (mm)
T	Mean annual temperature (°C)
ET°	Mean annual reference crop evapotranspiration (mm)
P/ET°	An agroclimatological index (–)
CCE	Calcium carbonate equivalent (%)
CEC	Cation exchange capacity ($cmol_c\ kg^{-1}$)
EC	Electrical conductivity ($dS\ m^{-1}$)
OC	Organic carbon (%)
D_{50}	Median grain size (μm)
TAFG	Total acidic functional group ($mmol\ g^{-1}$)
TBFG	Total basic functional group ($mmol\ g^{-1}$)
RD	Real density ($g\ cm^{-3}$)
SSA	Specific surface area ($cm^2\ g^{-1}$)
TPV	Total pore volume ($cm^3\ g^{-1}$)
TMV	Total micropore volume ($cm^3\ g^{-1}$)
APD	Average pore diameter (nm)
WDPT	Water drop penetration time (min)
MED	Molarity of ethanol droplet (M)
$\gamma_{90°}$	Ninety-degree surface tension ($mN\ m^{-1}$)
γ_s	Solid–air surface tension ($mN\ m^{-1}$)
θ	Solid–water contact angle (°)
FC	Field capacity ($cm^3\ cm^{-3}$)
PWP	Permanent wilting point ($cm^3\ cm^{-3}$)
HEMC	High energy moisture characteristic (–)
SWRC	Soil water retention curve (–)
BWRC	Biochar water retention curve (–)
PSD	Pore size distribution (–)
VDP	Volume of drainable pores ($cm^3\ cm^{-3}$)
MS	Modal suction (cm)
h	Matric suction (cm)
d	Diameter (μm)
θ	Volumetric water content ($cm^3\ cm^{-3}$)
θ_r	Residual water content ($cm^3\ cm^{-3}$)
θ_s	Saturated water content ($cm^3\ cm^{-3}$)
n	Shape parameter of van Genuchten[36] equation (–)
α	Scaling parameter of van Genuchten[36] equation (cm^{-1})
A	Quadratic coefficient of modified van Genuchten[36] equation (cm^{-2})
B	Quadratic coefficient of modified van Genuchten[36] equation (cm^{-1})
C	Quadratic coefficient of modified van Genuchten[36] equation ($cm^3\ cm^{-3}$)
PSL	Pore shrinkage line (–)
SI	Stability index (cm^{-1})
SR	Stability ratio (–)
SSI	Structural stability index (–)
PAW	Plant available water ($cm^3\ cm^{-3}$)
LLWR	Least-limiting water range ($cm^3\ cm^{-3}$)
IWC	Integral water capacity ($cm^3\ cm^{-3}$)
EI_{IWC}	Integral energy for IWC ($J\ kg^{-1}$)
PR	Penetration resistance (MPa)
b	Parameter of PR equation ($MPa\ cm^{-1}$)
c	Parameter of PR equation (–)
$\theta_{PR\text{-}2}$	Volumetric water content at critical penetration resistance ($cm^3\ cm^{-3}$)
$h_{PR\text{-}2}$	Matric suction at critical penetration resistance (cm)
$\theta_{A\text{-}10}$	Air-filled porosity of 10% ($cm^3\ cm^{-3}$)
$K_r(h)$	Mualem[50] relative hydraulic conductivity (–)
C(h)	Specific water capacity function ($\lvert d\theta/dh \rvert$) (cm^{-1})
p	Number of soil physical limiting factors (–)
ω	Weighting function of a limiting factor (–)
S	Dexter's index of soil physical quality (cm^{-1})
h_i	Matric suction at the inflection point (cm)

Annual removal of crop residues resulted in the depletion of soil organic carbon and led to soil degradation. However, agricultural residues should be directly returned and incorporated into the soil to manage it and increase the soil carbon pool. Due to the rapidly degradable nature of crop residues, their major part returns to the atmosphere through microbial respiration resulting in greenhouse gas emission and related environmental problems. Direct incorporation also can aggravate insect and plant diseases, which may result in additional pesticide application. Converting this lignocellulose material into biochar with an aromatic structure could be a win-win strategy to both sequestrate carbon and improve several soil quality parameters[1–3]. Accordingly, biochar amendment technology has been rapidly developed. Biochar is a kind of carbon-rich solid (usually 40–90%)

with a porous structure (porosity 70–90%) produced by controlled pyrolysis (zero or low oxygen environment) of biomass at temperatures above 250 °C and is distinguished from charcoal in its production process[4–6].

Soil physicochemical attributes directly affect soil productivity and crop production. Soil structure is one of the most important soil attributes since it affects soil moisture content, soil aeration, and soil temperature[7]. It also influences water, gases, heat, and material transformation within the soil profile. Furthermore, soil structure positively influences seed germination and root growth. Soil aggregates, as the basic units of soil structure, are secondary particles formed from the combination of the soil's primary mineral particles (i.e., clay, silt, and sand) and organic/inorganic substances[8]. Formation of soil aggregates is a function of physical forming forces (e.g., electrostatic, gravitational, and inter and intramolecular forces) between soil particles[9]; however, its stabilization is affected by external and internal factors, and their interactions[10]. One of the most influential factors affecting aggregation and consequently the structural stability of the soils is soil organic matter (SOM). Therefore, biochar as an organic matter substance can influence these soil properties[11]. Studies reported that biochar could improve various soil properties including soil structure[12,13] and soil aggregate stability[14–16]. Juriga and Simansky[8] stated that all mechanisms of aggregation and structure formation (i.e., the hierarchical theory of aggregation, the concentric theory, enhanced aggregation by precipitation of hydroxides, oxides, phosphates, and carbonates; aggregation resulting from cations-formed bridges between clay and SOM particles or their combinations) can be responsible for the formation and stabilization of soil structure after addition of biochar to the soils. In other words, biochar can be joined with mineral particles or part of the soil aggregates. Biochar contains base cations[17], which can be joined with clay and organic particles by cationic bridges[18], consequently creating a favorable soil structure condition. Biochar-associated multivalent ions may have a positive impact through interactions with negatively charged surface functional groups on organic matter (e.g., R-COO-) and soil minerals (e.g., Al-O-, Si-O-)[19]. The bridging effects of the multivalent ions (e.g., Fe^{3+}) may enhance the sorption of SOM onto clay minerals[20]. Furthermore, oxidation of the surface biochar particles may increase the content of carboxylic and hydroxylic functional groups which can adsorb clays and mineral soil particles and procedure macro-aggregates[12]. Šimanský[21] also reported that the application of 10 t ha^{-1} biochar increased the content of water-stable macro-aggregates in size fraction of 2 to 5 mm, but at the same time decreased 0.25 to 0.5 mm water-stable macro-aggregates; whereas, they observed that the application of 20 t ha^{-1} biochar had no significant effect. They concluded adding lower amounts of biochar may thus be more advantageous for soil aggregation than higher rates. Wang et al.[22] also reported that biochar enhances aggregation in their finer textured soil, with the mean 126% and 217% value increases in the mean weight diameter of soil aggregates for a walnut shell biochar gasified at 900 °C and a softwood biochar pyrolyzed at 600–700 °C with algal digestate, respectively. They concluded that the effects of biochar on soil aggregation and structural stability depend on the type of biochar and soil texture.

Biochar application has been also proposed to improve infiltration and water-holding capacity[23–27], enhance porosity, aggregation, and micropores[28–32], increase soil quality indices[3], and ameliorating soil hydrological characteristics under drought conditions[5]. Alterations of hydrological characteristics following biochar amendment seem to play a very important role in the nutrient and water dynamics towards plant roots, soil structure, and water-holding capacity of the soils[29]. Prior studies have noted the importance and utility of biochar to enhance soil water retention capacity[33]. In reviewing the literature, little data was found on the potential of this water to be used by plants[34,35]. The significance of biochar in promoting water retention and shallow slope stability was also demonstrated by Ng et al.[36]. They reported that the soil micropore increased by 22% in response to adding 0 to 10% biochar. Ng et al.[37] also stated that the grassed cover with 0 to 10% biochar could retain over four times higher negative pore-water pressure than the control (without biochar). They found that over 62% of total rainfall was evapotranspirated from biochar-amended covers, which was 10% larger than the biochar untreated cover. They also concluded that biochar resulted in a 13% reduction in infiltration; whereas, a 15% increase in water storage was observed. They recommended that 5% biochar content is sufficient to minimize water percolation.

Despite the results of previous studies regarding the influence of biochar on soil structure, water holding capacity, and their related soil attributes, there is little research about the effect of biochars produced at different pyrolysis temperatures on texturally different soils. Therefore, this work hypothesized that biochar application may have a considerable effect on soil structural stability, water availability, and distribution of soil pores, which in turn may affect integral energy (the energy required to take up a unit mass of soil water by a plant). Furthermore, we hypothesized that biochars produced at different pyrolysis temperatures have different effects on the mentioned attributes, particularly in various soils. Therefore, to address the hypothesis, we aimed to evaluate the effects of different levels of bagasse-derived biochar produced at different pyrolysis temperatures on (i) possible changes in structural stability through measuring the water retention curve at high matric potential and evaluating a new dimensionless index based on the data of the water retention curve; (ii) some thermodynamic, physical, biological, and chemical aspects of aggregation; (iii) various water availability parameters, different in the factors that limit plant growth and reducing the restriction of high soil mechanical resistance to water uptake by plants; and (iv) geometry of the pore size distribution curve (PSD) to describe the mechanisms of transportation of fine biochar particles within soil porous medium.

Materials and methods

Soils: preparation, analysis, and the climatic conditions of the regions

The experiment was performed in a greenhouse at the College of Agriculture, Shiraz University, Shiraz, Iran. Studied soils were collected from the topsoil (0- to 20-cm depth) of the three different soils including a silty-clay Inceptisols (SCInc), a silty-clay-loam Alfisols (SCLAlf), and a loam Aridisols (LArid) based on Khormali[38]. The soils located respectively in Ardakan (30.2425° N 51.9924° E), Khosrow Shirin (30.9049° N 52.6921° E), and Soormagh (31.0356° N 52.8393° E). The climatic data of the studied regions are presented in Table 1. Three considered locations differed in terms of P/ET_0 (i.e. ratio of mean annual precipitation to mean annual reference

Area/soil	P (mm)	T (°C)	ET0 (mm)	P/ET0 (–)	Soil water/ temperature regime
Climatic data and moisture and temperature regimes					
Ardakan	609	12.4	1000	0.60	Xeric/Mesic
Khosrow Shirin	342	12.1	1000	0.35	Xeric/Mesic
Soormagh	149	13.6	1500	0.10	Aridic/Mesic
	CCE (%)	CEC ($cmol_c\ kg^{-1}$)	pH (–)	EC ($dS\ m^{-1}$)	OC (%)
Chemical properties					
SCInc	33.3	17.6	7.6	0.5	0.8
SCLAlf	30.5	16.4	7.7	0.9	0.8
LArid	46.4	8.7	8.0	1.6	0.2

Table 1. Climatic data and water and temperature regimes of the areas where soils were collected after Khormali[38] and initial chemical properties of the soils used for the experiment. P, mean annual precipitation; T, mean annual temperature; ET0, mean annual reference potential evapotranspiration; P/ET0, agroclimatological index. CCE, calcium carbonate equivalent; CEC, cation exchange capacity; EC, electrical conductivity; OC, organic carbon.

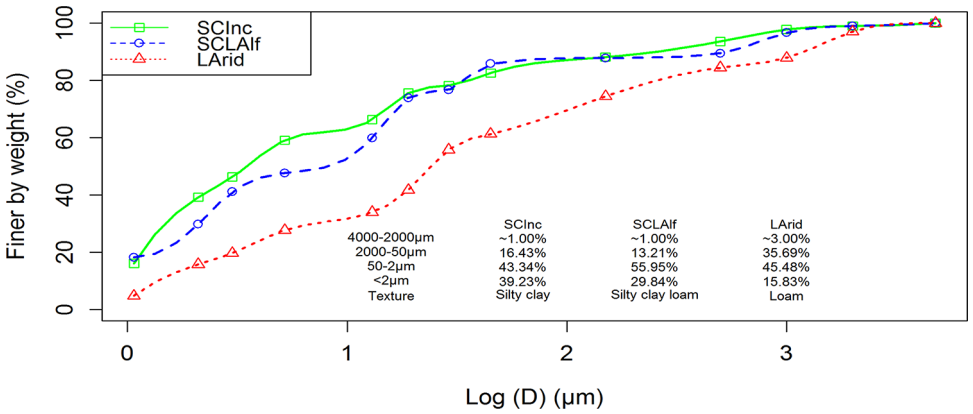

Fig. 1. Grain-size distribution (GSD) curves of the initially studied soils.

potential evapotranspiration) index. The P/ET_0 index is an important agricultural and biological criterion for crop growth in arid and semi-arid regions as well as a reliable weathering index based mainly on climatic factors for soil development and mineral transformation. The variation of the P/ET_0 index is in accordance with the soil water and temperature regimes[38]. The soils were first air-dried, homogenized, and then passed through a 4 mm sieve. The mechanical or sieve analysis was used to determine the distribution of the larger-sized particles (0.05 to 4 mm diameter) and the hydrometer method for determining the finer particles (< 0.05 mm diameter) according to ASTM D422-63[39]. Grain-size distribution (GSD) curves of the studied soils are shown in Fig. 1. In Table 1, some basic chemical properties of the initial (untreated) soils are presented.

Biochars: preparation and characterization

The biochar feedstock was sugarcane bagasse (BG) prepared from the Imam Khomeini sugar factory, Khuzestan, southwest Iran. The water content of biomass plays a vital role in pyrolysis processes. Before the pyrolysis, raw precursors were dried in an electric oven at 110 °C for 24 h to remove the excess water. Biochar was produced in a muffle furnace at a low-oxygen environment by applying double aluminum foil at two different low (300 °C) and high (600 °C) pyrolysis temperatures with a 10 °C min^{-1} heating rate and 4 h residence time. After pyrolysis, the resultant biochars (BC300 and BC600) were cooled to diminish rapid oxidation (leading to more product homogeneity) and auto-ignition. According to sieve analysis, all biochar samples had a median grain size (D_{50}) of about 50 microns. The detailed descriptions of the organo-chamical and hydro-physical properties of the biochars have been brought by Moradi-Choghamarani et al.[40,41]. Table 2 summarizes some basic physical and chemical properties of the biochars.

Preparation of experimental treatments

Three sets of test substrates based on soil types were prepared. Each set consisted of about 15 kg air-dried soil amended with four doses (0 (control), 1, 2, and 3 %w/w equal to 0, 20, 40, and 60 ton ha^{-1}; labeled as 0BC, 1BC, 2BC, and 3BC, respectively) of two sugarcane bagasse-derived biochars produced at 300 °C and 600 °C (BC300 and BC600, respectively). For instance, SCInc-3BC300 represents amending a silty-clay Inceptisol with 3 w/w% of the biochar produced at 300 °C. Biochar-treated soils were transferred to plastic containers (pots with 29 cm

Biochars	EC (dS m^{-1})	CEC ($cmol_c$ kg^{-1})	TAFGs (mmol g^{-1})	TBFGs (mmol g^{-1})	RD (g cm^{-3})	SSA (cm^2 g^{-1})	TPV (cm^3 g^{-1})	TMV (cm^3 g^{-1})	APD (nm)
Physicochemical properties									
BC300	1.2[a]	105.3[a]	9.0[a]	0.8[b]	1.4[b]	6.9[b]	0.014[b]	0.003[b]	25.1[a]
BC600	1.7[a]	18.4[b]	5.8[b]	4.1[a]	1.6[a]	99.1[a]	0.069[a]	0.045[a]	7.5[b]

	WDPT (min)	MED (M)	γ_{90° (mN m^{-1})	γ_s (mN m^{-1})	θ (°)
Wettability assessment					
BC300	immediately	0	72.1	18.0	< 90
BC600	immediately	0	72.1	18.0	< 90

Table 2. Some basic physicochemical properties and wettability assessment of biochars used for the experiment prepared at 300 °C and 600 °C (BC300 and BC600) after Moradi-Choghamarani et al.[40,41]. EC, electrical conductivity; CEC, cation exchange capacity; TAFG, total acidic functional groups; TBFG, total basic functional groups; RD, real density; SSA, specific surface area; TPV, total pore volume; TMV, total micropore volume; APD, average pore diameter; WDPT, water drop penetration time; MED, the molarity of ethanol droplet; γ_{90°, ninety-degree surface tension; γ_s, solid–air surface tension; θ, solid–water contact angle. EC was measured in a 1:20 ratio of biochar:deionized water. For each parameter, values followed by the same lower-case letters are not significantly different ($p < 0.05$) according to the least significant difference (LSD) test.

and 18 cm in top and bottom diameters, respectively, and 26.2 cm in height) with a layer of gravel at the bottom to facilitate drainage. The experiment was carried out under greenhouse conditions with three replications. Treated soils were incubated for 540 days at a controlled temperature of 22 ± 2 °C, relative humidity of 65 ± 5%, and soil moisture of field (pot) capacity, FC conditions. The presence of water has a leading role in biochar weathering in the soil through processes such as dissolution, hydrolysis, carbonization and decarbonization, hydration, and redox reactions, as well as interactions with soil biota[42]. Accordingly, each container was watered with a constant amount of tap water approximately equivalent to its field capacity (FC), that has been measured by a pressure plate apparatus before starting the experiment and maintained at this water condition by adding water to a constant weight. However, once every 60 days the pots were allowed to experience a short-term drought due to the important role of the meniscus force which can rearrange the internal orientation of grains and form aggregates[25].

Structural stability

In this study, the high energy moisture characteristic (HEMC) method was applied to investigate soil aggregate stability[29,42–44]. In this method, changes in soil pore size distribution (PSD) are followed to determine a structural index (SI) after the accurately controlled wetting process to ensure that hydration energy and entrapped air are responsible for the aggregate breakdown. Briefly, two separate batches of aggregates were placed in steel cores of 50 mm in diameter and height and then wetted from the bottom either slowly or rapidly in a controlled manner. After that, their soil water retention curves (θ = f (h), SWRC) at high energies of water tension (h) from 0 to 50 cm with 5 cm intervals and equilibration time of 24 h for each tension value, corresponding to drainable pores of 600 to 60 µm in diameter, were measured using the sandbox apparatus. The bottom of the steel cylinders was previously covered by a porous membrane. For rapid wetting, the cores were placed in distilled water and left submerged for 24 h. For slow wetting, the cores were placed in a sandbox and saturated from 50 to 0 cm water tension with an equilibration period of 24 h for each tension value. The gravimetric water content (w, g g^{-1}) was determined when the samples were oven-dried at 105 °C for 24 h after the last equilibrium water tension. The gravimetric water contents were then converted to volumetric water contents (θ, cm^3 cm^{-3}) by multiplication to their corresponding bulk density values.

For a given wetting rate, the SI is defined as the ratio of the volume of drainable pores (VDP) to modal suction (MS)[42].

$$\mathrm{SI} = \mathrm{VDP}/\mathrm{MS} \tag{1}$$

where the MS (cm) corresponds to the water tension (h, cm) at the peak of the specific water capacity curve ($C(\theta) = |d\theta/dh|$, cm^{-1}); it can be calculated by equating the second derivative of the water retention equation to zero and the VDP (cm^3 cm^{-3}) is defined as the integral of the area under the specific water capacity curve and above its baseline. In other words, MS is the value of h that is associated with the most common pore size diameter. The following parametric model described by van Genuchten[45] traditionally is used by many researchers to model the shape of SWRC:

$$\theta = \theta_r + \left[(\theta_s - \theta_r)(1 + (\alpha h)^n)^{-m}\right] \tag{2}$$

where the subscripts r and s denoted residual and saturated water content (cm^3 cm^{-3}), respectively; h is water tension (a positive quantity, cm); α (> 0, in cm^{-1}) and n (> 1, dimensionless) control position and steepness of SWRC, respectively. Small m (m = 1-(1/n)) values are associated with soils that have a wide PSD. In practice, m ranges between 0.1 and 0.9[46]. When the van Genuchten[45] equation is used for modeling the HEMC data (θ, h), it cannot accurately predict the sloping legs of HEMC data thus overestimating the VDP and subsequently the

SI. However, saturated and residual water contents and therefore MS can be accurately predicted by fitting van Genuchten's[45] model to the HEMC data. To overcome this problem, it is suggested to model the shape of SWRC by the following modified van Genuchten[45] equation[43]:

$$\theta = \theta_r + \left[(\theta_s - \theta_r)(1 + (\alpha h)^n)^{-m}\right] + Ah^2 + Bh + C \tag{3}$$

where θ_s and θ_r cannot be physically interpreted in terms of saturated and residual water contents and is generally known as the pseudo residual and saturated water contents ($cm^3\ cm^{-3}$) for HEMC data. A (cm^{-2}), B (cm^{-1}), and C ($cm^3\ cm^{-3}$) are quadratic coefficients to better fit the HEMC data. The specific water capacity function is computed by differentiating Eq. (3) for h as follows:

$$C(\theta) = |d\theta/dh| = \alpha mn(\theta_s - \theta_r)(\alpha h)^{n-1}(1 + (\alpha h)^n)^{-m-1} - 2Ah - B \tag{4}$$

The VDP ($cm^3\ cm^{-3}$) was calculated as follows:

$$VDP = \int_{h_1}^{h_2} (C(\theta) - PSL)\, dh \tag{5}$$

where PSL is the baseline term which is called the pore shrinkage line ($2Ah + B$) and h_1 and h_2 are points of intersection. The PSL represents the rate of water loss due to aggregate shrinkage rather than pore emptying[44].

The MS (cm) was calculated as:

$$d^2\theta/dh^2 = (\theta_s - \theta_r)\left[-\alpha^2(-m-1)mn^2(\alpha h)^{2n-2}(1 + (\alpha h)^n)^{-m-2} - \alpha^2 m(n-1)n(\alpha h)^{n-2}(1 + (\alpha h)^n)^{-m-1}\right] + 2A = 0 \tag{6}$$

According to Hosseini et al.[44], the following approximate equation will be derived from Eq. (6) by assuming the negligible effect of the $2A$ term due to the very low value of A:

$$MS \approx \frac{1}{\alpha}\left(\frac{n-1}{n}\right)^{1/n} \tag{7}$$

Dividing SI indices [Eq. (1)] obtained from the fast and slow wetting yields the dimensionless stability ratio (SR):

$$SR = \frac{SI_{FW}}{SI_{SW}} \tag{8}$$

The SR is the aggregate stability on a scale of zero to one (the closer the SR value is to 1, the greater soil structural stability)[44]. We introduced the dimensionless structural stability index (SSI) as below:

$$SSI = \frac{VDP_{FW}}{VDP_{SW}} + \frac{MS_{SW}}{MS_{FW}} \tag{9}$$

The SSI value closer to two indicates greater structural stability.

All calculations (including model parameter optimization, etc.) were performed using R programming language version 3.6.3 (https://www.r-project.org).

Soil water availability

Various definitions in the literature indicate the soil's available water for plant uptake. The well-known conventional plant available water (PAW, $cm^3\ cm^{-3}$) was calculated as the difference between FC (h of 330 cm) and PWP (h of 15000 cm), which themselves had been measured using a pressure plate apparatus. One major drawback of this approach is that it considers just water potential as a restricting factor. Therefore, it is based completely on uniform water absorption by plants in a cut-off form from FC to PWP[47]. The term least limiting water range (LLWR, $cm^3\ cm^{-3}$) considers three main plant growth-limiting factors (i.e. water potential, aeration, and penetration resistance) and integrates them into a single parameter. To obtain the LLWR, the results obtained from SWRC and penetration resistance (PR) curves were considered. de Lima et al.[47] coded a *soilphysics* package in the R environment for the calculations of plant available water quantities. In their package, to consider water potential restriction, de Lima et al.[47] used the exponential water retention equation presented by Ross et al.[48]. In the current study, van Genuchten's[45] equation was fitted to water retention data of the control and biochar-treated soils due to its better performance which causes more accurate calculations. A power model was employed to make a continuous function of soil penetration resistance (PR, MPa) vs. h (cm) to consider PR limitation:

$$\mathrm{PR} = \mathrm{bh}^{\mathrm{c}} \tag{10}$$

where b (MPa cm^{-1}) and c are empirical fitting parameters[49]. The soil PR data were taken using a pocket penetrometer (ELE international 29-3729, Soiltest Inc.) at six h values of 110, 330, 3000, 7000, 11,000, and 15,000 cm. The final PR value was considered as the average of the three replicates. The water content (θh_{PR-2}, cm) and equivalent matric suction (h_{PR-2}, cm) at which PR reaches the critical point of 2 MPa were calculated according to Eqs. (10) and (2). In connection with aeration restriction, the water content at an air-filled porosity of 10% (θ_{A-10}, $cm^3\ cm^{-3}$) was calculated using the following equation:

$$\theta_{A-10} = \left(1 - \frac{BD}{RD}\right) - 0.1 \tag{11}$$

where BD and RD are bulk and real (particle) densities (g cm^{-3}), respectively. In a cut-off form, the upper limit of LLWR was considered as the water content at FC or at θ_{A-10}, whichever is the smaller. For the lower limit of LLWR, θ_{PR-2} or PWP is the growth-limiting factor, and the larger was considered as the lower limit of LLWR. Groenevelt et al.[49] considered the sharp cut-off between two points in PAW and LLWR procedures as a defect and introduced the term integral water capacity (IWC, cm^3 cm^{-3}) to generalize the availability of soil water with its limiting factors as a continuous weighting function. The equation presented by Groenevelt et al.[49] to calculate IWC is as follows:

$$IWC = \int_0^{\infty} \left(\prod_{i=1}^{p} \omega_i(h)\right) C(h)dh \tag{12}$$

where C(h) is the absolute specific water capacity function (i.e., $|d\theta/dh|$, cm^{-1}) according to the van Genuchten[45] equation and $\omega_i(h)$ are *multiplicative* weighting functions accounting for the first to p^{th} limiting soil physical properties as a function of h. High soil hydraulic conductivity along with lack of oxygen at the wet range and low soil hydraulic conductivity and high resistance to penetration at the dry range are considered as restriction factors to water uptake by plants. The relative hydraulic conductivity equation of Mualem[50] was used in IWC calculation:

$$K_r(h) = \left[1 - (\alpha h)^{n-1}\left[1 + (\alpha h)^n\right]^{\left(\frac{1}{n}-1\right)}\right]^2 \left[1 + (\alpha h)^n\right]^{\left(\frac{1-n}{2n}\right)} \tag{13}$$

where $K_r(h)$ is the relative hydraulic conductivity.

The amount of energy required to remove the available water value defined by IWC (EI_{IWC}, J kg^{-1}) was computed based on the modified and generalized method proposed by Minasny and McBratney[51]:

$$EI_{IWC} = \frac{1}{10IWC}\int_{h_i}^{h_f} \left(\prod_{i=1}^{m} \omega_i(h)\right) hC(h)dh \tag{14}$$

where EI_{IWC} is the integral energy for the IWC and h_i and h_f are boundary matric suctions (cm) at the wet and dry ends, respectively. For details on the procedures and equations, we refer readers to Groenevelt et al.[49], Minasny and McBratney[51], Asgarzadeh et al.[52,53], and de Lima et al.[47]. All calculations were performed using R programming language version 3.6.3 (https://www.r-project.org).

Pore size distribution (PSD) and S-index

Soil water retention data were taken by combining the results from the sandbox test (up to a pressure head of 100 cm) and pressure plate extractor (from 300 to 15000 cm) following ASTM D6838-02 as described in the literature[54]. The undisturbed substrate samples were previously saturated on the sand bed by capillary rise and then equilibrated at a wet-to-dry sequence of thirteen applied tensions (h) including 5, 10, 15, 20, 25, 30, 35, 40, 45, 50, 70, 90, and 110 cm. Determination of the SWRC was continued pneumatically with pressure plate extractor at 300, 1000, 3000, 5000, 7000, 9000, 11,000, 13,000, and 15,000 cm tensions. After equilibrium at each h value, soil samples were weighted and the next h was applied. The gravimetric water contents (w, g g^{-1}) were determined when the samples were oven-dried at 105 °C for 24 h after the last equilibrium water tension and then converted to volumetric water contents (θ, cm^3 cm^{-3}) using bulk density values of the soils. Water tensions (h, cm) were converted to the equivalent pore diameter (d, μm) using the Young-Laplace relation d = 2980/h[55] and then soil PSD curves were obtained as dθ/d(ln h) versus ln (d) by fitting a cubic spline function directly coded in R programming language (R 3.4.3) as described in the previous kinds of literature[56,57].

S parameter is a soil physical quality index obtained from the slope of the SWRC at the inflection point[58]:

$$S = d\theta/dln(h) = -n(\theta_s - \theta_r)[(2n-1)/(n-1)]^{[(1/n)-2]} \tag{15}$$

Statistical analysis

A factorial arrangement was used for the 72 treatments (4 biochar doses × 3 soil types × 2 pyrolysis temperatures) and three replications. Three-way analysis of variance (ANOVA) was applied to determine the effect of soil type, biochar type, application rate, and their interactions on the studied soil properties. The treatment means were compared using the least significant difference (LSD) test at the probability level of 0.05. All statistical analyses were performed using SAS software version 9.1 (SAS Institute, Cary, NC). Plotting, fitting, and parameterization, as well as calculations of errors, were performed using R software version 3.6.1 (https://www.r-project.org).

Results and discussion

Properties of the studied soils of different regions

As shown in Table 1, among the following places, the long-term mean annual precipitation is in order SCInc > SCLAlf > LArid, with values of 609 mm, 342 mm, and 149 mm, respectively. The opposite pattern is true for the mean annual temperature. There was a similar trend for both mean annual precipitation and P/ET_0. SCInc and SCLAlf soils have been developed under a Xeric moisture regime with calcareous alluvium parent

material. LArid is characterized by the Aridic soil moisture regime with calcareous and gypsiferous alluvium parent material[38]. Soils were commonly calcareous with relatively low OC (Table 1). OC in SCInc and SCLAlf soils is fourfold higher than that of Larid due to higher precipitation and, consequently a higher plant cover. The soils were ranked as SCInc > SCLAlf > LArid in terms of their clay contents (Fig. 1). In other words, in this study SCInc that contains nearly 40% clay named as fine-textured soils proposed by USDA[59]. The SCInc and SCLAlf soils are dominated by chlorite, illite, kaolinite, vermiculite, and smectite clay minerals; whereas, the LArid soil is dominated by chlorite, illite, and palygorskite[38]. In general, SCInc and SCLAlf soils have smaller GSD when compared with LArid (Fig. 1) owing to higher percentages of clay particles. Therefore, cation exchange capacity (CEC), which is a measure of the adsorption of exchangeable cations on the negatively charged surface of soil colloids, follows a pattern similar to that of OC and clay contents, with values of 17.6, 16.4, and 8.7 $cmol_c\ kg^{-1}$ for SCInc, SCLAlf, and LArid, respectively.

Biochar properties as influenced by pyrolysis temperature

Some properties of bagasse-derived biochars used for this experiment are tabulated in Table 2. In comparison with BC300, biochar produced at high temperature (BC600) has higher electrical conductivity (EC), total basic functional groups (TBFGs), real density (RD), specific surface area (SSA), total pore volume (TPV), and total micropore volume (TMV). In general, BC300 has higher CEC and total acidic functional groups (TAFGs) than that of BC600 (Table 2). BC300 and BC600 had SSA of 6.9 $m^2\ g^{-1}$ and 99 $m^2\ g^{-1}$, respectively. Other investigators also reported that increasing pyrolysis temperature causes changes in biochar SSA and porosity[60–62] most likely due to the decomposition of organic matter and formation of micropores[63]. Furthermore, exposure of the aromatic lignin core and destruction of ester and aliphatic alkyl groups at higher pyrolysis temperatures may result in increased SSA[64]. Pore-blocking substances are driven off or are thermally cracked with increasing pyrolysis temperature, causing an increase in the externally accessible surface area[65]. Furthermore, pyrolysis may increase the SSA and pore volumes through progressive degradation of the organic materials (cellulose, lignin) and the formation of vascular bundles or channel structures[66,67]. In their review, Alghamdi[4] also ranged SSA of different biochar types from 1.4 $m^2\ g^{-1}$ to 500 $m^2\ g^{-1}$. Our results were in accordance with the findings of other investigators. So that, our mentioned lower and upper boundaries were also reported by Li et al.[68] in pyrolysis pine sawdust at a temperature of 300 °C and by Suliman et al.[69] in pyrolysis Douglas fir wood at a temperature of 600 °C, respectively. The higher the pyrolysis temperature, the smaller the pore size distribution. The average pore diameter (APD) of BC300 was about 3 times larger than that of BC600 (25.1 nm for BC300 and 7.5 nm for BC600). Both BC300 and BC600 are classified as mesoporous materials based on the IUPAC classification. In this classification, a mesoporous material is a material containing pores with diameters between 2 and 50 nm. Such pores are equivalent to water suctions of 29,800 to 745,000 cm and are not available for plant use. Small diameter pore fractions increase with the increase in pyrolysis temperature[70]. Ghorbani et al.[62] also reported that there is a positive correlation between organic functional groups (OFGs) and SSA and pure volumes of biochars. They also stated that the higher micro-pores pores which resulted from high pyrolysis temperature cause an extended SSA. Both BC300 and BC600 have a hydrophilic surface (Table 2). For details about various physic-chemical properties of the studied biochars, we refer readers to Moradi-Choghamarani et al.[40,41]. Particle surface characteristics such as SSA and surface functionality play a key role in driving organo-mineral interactions, thereby affecting soil aggregation and water retention behavior. But then the surface chemical/molecular properties of biochar will change when treated with soil minerals. Zhao and Zhou[71] indicated that mineral (soil) treatment increased the micropore and mesopore surface area, pore diameter, and pore volume of biochar particles. Accumulation of carbonates in the pores of mineral-treated biochar of calcareous soils and deposition/precipitation of a layer of either oxy-hydroxides of Fe and Al on part of the biochar surface has been reported[42]. Zhao and Zhou[71] stated that clay mineralogy and biochar production temperature can affect the rate of such changes. They also pointed out that in comparison with original wheat straw-derived biochars, mineral-treated biochars have greater electron-donating capacity, double-bond equivalent, phenolic group, and polarity.

Structural stability

Results of the effect of applied biochars on the structural stability of the studied soils are presented in Table 3. SR and SSI were significantly affected by different doses of biochar application and soil types (Table 3). Values of SR and SSI (Table 4) in SCInc soil amended with 0, 1, 2, and 3% of BC300 had a relative magnitude of 1:1.09:1.21:1.53 and 1:1.02:1.11:1.20, respectively; highlighting an increase in aggregate stability with increasing the amount of applied biochar probably because they play a role of binding agent between soil particles. There was a positive and significant correlation ($r = 0.93$, $p < 0.01$) between SSI and SR (data not shown). Besides, VDP and MS differed significantly among soil types and were significantly affected by the interaction between soil type and application rate of biochar (Table 3). There was no significant difference in VDP, MS, SR, and SSI between BC300 and BC600. However, SI indicated significant differences between almost all of the treatments and the interactions between them (Table 3). Nonetheless, we believe that the SI appears not to exhibit admissible results as an index in the investigation of soil aggregate stability. Uncertainty still prevails about the ability of biochar to promote aggregation through the union of primary particles in aggregates and the resistance of aggregates to disrupting agents (e.g., raindrops, slaking, mechanical plowing, etc.). Some investigators reported positive effects[18,23] and others negative[72,73] or neutral[1,74]. In their review, Alghamdi[4] ranged the percentage increment in aggregate stability of biochar-amended soils from 6 to 216%. In the current study, the significant increase in soil aggregate stability regarding the SR ranged from 35% in LArid-2BC600 to 100% in SCLAlf-3BC600. Biochar increased VDP and decreased MS in SCInc and SCLAlf soils (Table 4). By contrast, VDP decreased and MS increased with increasing doses of both applied biochars in LArid soil because of the infilling of macro-pores by the fine biochar particles. This re-configured pore geometry in coarse-textured soils is advantageous in raising water retention capacity and reducing the frequency and cost of irrigation.

Source of variation	Degree of freedom	Properties							
		VDP		MS		SI			
		Fast	Slow	Fast	Slow	Fast	Slow	SR	SSI
Soil (S)	2	20.71***	61.18***	1.74	3.87*	84.26***	55.86***	4.43*	7.70**
Biochar (BC)	1	0.31	0.58	0.26	0.58	4.55*	3.10	0.43	1.64
Rate (R)	3	1.78	1.27	0.64	1.61	3.03*	3.17*	11.00***	13.21***
S×B	2	0.65	1.08	2.18	2.42	8.52**	2.65	0.21	0.32
S×R	6	3.79**	4.51**	3.74**	5.80**	33.24***	13.66***	1.35	0.31
B×R	3	0.58	0.34	0.06	0.13	3.93*	1.23	1.18	0.48
S×B×R	6	0.35	0.66	0.47	0.71	3.98**	1.54	0.41	0.38
CV (%)		45.55	30.55	22.32	23.51	23.34	41.16	23.77	10.43

Table 3. The *F* ratios of analysis of variance (ANOVA) for the effects of four rates of two applied biochars on volume drainable pore (VDP, $cm^3\ cm^{-3}$), modal suction (MS, cm), structural index (SI, cm^{-1}), stability ratio (SR), and structural stability index (SSI) of three different studied soil types. CV, Coefficient of variation. *,** and ***Indicate significant effects at the probability levels of 0.05, 0.01, and 0.001, respectively.

Soil	Biochar	Rate (%wt)	VDP		MS		SI		SR	SSI
			Fast	Slow	Fast	Slow	Fast	Slow		
SCInc	BC300	0	0.036^{c}	0.092^{c}	18.93^{a}	18.81^{a}	0.0018^{c}	0.0053^{a}	0.34^{b}	1.24^{b}
		1	0.037^{bc}	0.106^{b}	17.91^{a}	17.07^{a}	0.0019^{c}	0.0060^{a}	0.37^{b}	1.26^{b}
		2	0.044^{b}	0.096^{bc}	17.78^{a}	17.04^{a}	0.0024^{b}	0.0055^{a}	0.41^{ab}	1.38^{ab}
		3	0.064^{a}	0.118^{a}	17.14^{a}	17.40^{a}	0.0034^{a}	0.0067^{a}	0.52^{a}	1.49^{a}
	BC600	0	0.036^{d}	0.092^{b}	18.93^{a}	18.81^{a}	0.0018^{b}	0.0053^{b}	0.34^{b}	1.24^{b}
		1	0.047^{c}	0.124^{ab}	17.45^{ab}	17.44^{a}	0.0036^{ab}	0.0110^{a}	0.34^{b}	1.29^{b}
		2	0.060^{b}	0.124^{ab}	13.94^{ab}	13.52^{b}	0.0042^{a}	0.0091^{a}	0.45^{ab}	1.43^{ab}
		3	0.074^{a}	0.129^{a}	12.44^{b}	11.57^{b}	0.0043^{a}	0.0072^{a}	0.58^{a}	1.58^{a}
SCLAlf	BC300	0	0.019^{c}	0.059^{d}	18.31^{a}	17.08^{a}	0.0009^{b}	0.0032^{d}	0.29^{a}	1.22^{b}
		1	0.045^{bc}	0.096^{c}	12.87^{ab}	11.08^{b}	0.0032^{b}	0.0084^{c}	0.37^{a}	1.27^{b}
		2	0.084^{a}	0.181^{a}	11.93^{b}	10.34^{b}	0.0066^{a}	0.0183^{a}	0.39^{a}	1.28^{b}
		3	0.073^{ab}	0.117^{b}	11.66^{b}	9.81^{b}	0.0065^{a}	0.0112^{b}	0.55^{a}	1.50^{a}
	BC600	0	0.019^{bc}	0.059^{a}	18.31^{a}	17.08^{a}	0.0009^{b}	0.0032^{b}	0.29^{a}	1.22^{b}
		1	0.010^{c}	0.031^{a}	17.15^{a}	16.54^{a}	0.0006^{b}	0.0019^{b}	0.32^{a}	1.29^{b}
		2	0.047^{b}	0.075^{a}	14.11^{b}	12.16^{b}	0.0032^{b}	0.0059^{b}	0.57^{a}	1.54^{b}
		3	0.092^{a}	0.121^{a}	12.61^{b}	11.41^{b}	0.0074^{a}	0.0125^{a}	0.58^{a}	1.56^{a}
LArid	BC300	0	0.137^{ab}	0.311^{b}	11.51^{b}	7.52^{b}	0.0120^{ab}	0.0490^{a}	0.26^{c}	1.04^{b}
		1	0.193^{a}	0.380^{a}	12.16^{b}	8.30^{b}	0.0162^{a}	0.0536^{a}	0.31^{bc}	1.17^{ab}
		2	0.117^{ab}	0.232^{b}	17.29^{a}	13.92^{ab}	0.0068^{b}	0.0177^{a}	0.35^{ab}	1.28^{ab}
		3	0.079^{b}	0.215^{b}	18.25^{a}	18.28^{a}	0.0042^{b}	0.0119^{a}	0.38^{a}	1.30^{a}
	BC600	0	0.137^{ab}	0.311^{a}	11.51^{c}	7.52^{c}	0.0120^{a}	0.0490^{a}	0.26^{b}	1.04^{b}
		1	0.150^{a}	0.359^{a}	15.61^{b}	13.15^{b}	0.0096^{ab}	0.0296^{a}	0.33^{ab}	1.23^{ab}
		2	0.115^{b}	0.218^{b}	19.65^{a}	16.25^{ab}	0.0055^{bc}	0.0143^{a}	0.38^{a}	1.31^{a}
		3	0.073^{c}	0.189^{b}	21.19^{a}	19.45^{a}	0.0033^{c}	0.0094^{a}	0.35^{a}	1.31^{a}

Table 4. Mean comparisons of structural stability parameters including volume drainable pore (VDP, $cm^3\ cm^{-3}$), modal suction (MS, cm), structural index (SI, cm^{-1}), stability ratio (SR), and structural stability index (SSI) for three different soil types amended with two sugarcane bagasse-derived biochars produced at 300 °C and 600 °C and four biochar application rates. For each attribute, means correspond to various levels of each applied biochar (in each column) followed by the same lowercase letters are not significantly different ($p < 0.05$) based on the LSD test.

In connection with changes in aggregation following the incorporation of soil amendments based on the literature review, it would be more useful if thermodynamical, physical, biological, and chemical aspects were investigated separately. Biomass converted to biochar is still thermodynamically unstable under the oxidative conditions of most surface soils. Subsequently, the entropy and the enthalpy of the new environment (soil-biochar) change continuously and go from one steady state to another[42]. From a physical point of view, the biochar particles, due to their fine sizes, fine pore structure (intra pores within biochar), high SSA, and high

Source of variation	Degree of freedom	Properties				
		PAW	LLWR	IWC	EI_{IWC}	FC
Soil (S)	2	11.21***	48.06***	32.31***	17.47***	37.66***
Biochar (B)	1	2.85	1.87	0.1	3.37	3.28
Rate (R)	3	10.95***	3.93*	5.04**	57.81***	27.03***
S×B	2	1.47	5.02*	1.66	0.41	0.75
S×R	6	11.13***	22.00***	2.51*	1.81	1.63
B×R	3	1.19	1.36	0.21	2.21	0.59
S×B×R	6	0.29	1.81	0.24	0.61	0.21
CV (%)		20.64	13.16	25.92	21.42	14.95
		Properties				
		PWP	h_{PR-2}	θ_{A-10}	S	h_i
Soil (S)	2	121.72***	84.32***	1.83	2.29	1.10
Biochar (B)	1	3.22	2.17	0.01	1.93	18.75***
Rate (R)	3	91.99***	33.22***	6.52**	4.25**	1.05
S×B	2	4.05*	2.31	0.05	0.42	5.53**
S×R	6	2.98*	2.67*	0.18	1.27	50.25***
B×R	3	0.47	0.47	0.01	0.94	2.55
S×B×R	6	0.54	0.81	0.04	0.46	0.76
CV (%)		13.47	17.22	15.11	18.99	17.31

Table 5. The *F* ratios of analysis of variance (ANOVA) for the effects of four rates of two applied on soil water available attributes of three different studied soil types. PAW: plant available water ($cm^3\ cm^{-3}$); LLWR: least limiting water range ($cm^3\ cm^{-3}$); IWC: integral water capacity ($cm^3\ cm^{-3}$); EI_{IWC}: integral energy calculated for IWC; FC: field capacity ($cm^3\ cm^{-3}$); PWP: permanent wilting point ($cm^3\ cm^{-3}$); h_{PR-2}: matric suction at which soil penetration resistance reaches the critical value of 2 MPa (cm); θ_{A-10}: water content at an air-filled porosity of 10% ($cm^3\ cm^{-3}$); S: Dexter's index of soil physical quality (cm^{-1}); h_i: matric suction at the inflection point of semi-logarithmic water retention curve (cm). *,** and ***indicate significant effects at the probability levels of 0.05, 0.01, and 0.001, respectively.

surface functional groups act similarly to clay particles in raising the air-water menisci with increasing matric suction. Consequently, more contracting forces are exerted on particles to move, rearrange, and rebound until entropy is minimized. From a biological point of view, researchers have to study the adhesive properties of organic compounds resulting from the decomposition of biochar grains by soil organisms. Adhesive molecules such as microbial polysaccharides of bacterial and fungal origin and animals such as earthworms may contribute to the adhesion of mineral particles. Furthermore, they may act as substrates and influence microbial community dynamics[75]. Some investigators[4] reported that oxidation of labile biochar components (aliphatic carbon) by the soil microorganisms enhances the excretion of mucilage, which, in turn, adheres to soil particles and builds stable soil aggregates. It would be interesting to recognize such components and assess their adhesive effects to collect mineral particles. From a chemical point of view, researchers need a molecular picture of biochar-soil mineral interactions. The surface molecular properties of biochar particles and soil minerals determine the bonds that hold them together. A good illustration of this is the research conducted by Newcomb et al.[76], which found COO^- as the strongest binding energy of soil organic matter on the mica surface. Adsorption of dissolved organic matter, biopolymers, and low molecular weight compounds present in biochar onto the soil minerals[42] (Zhao and Zhou[71]) also can affect biochar-mineral complex. The secondary silicates and hydrous metal oxide, particularly those that are poorly crystalline or amorphous, are responsible for soil reactivity. They can form strong surface complexes with both inorganic and organic species. The chemistry of the local environment also is important in driving organo-mineral interactions. For example, Juriga Newcomb et al.[7] proved that ionic strength and pH of soil solution could play a direct role in the adhesion of organic matter to mineral surfaces. More broadly, research is also needed to determine the mechanisms governing biochar-soil mineral interactions.

Soil water availability

The PAW, LLWR, and IWC of the substrates significantly depended on the soil type and rate of biochar amendment (Table 5). Biochar addition significantly decreased PAW, LLWR, and IWC in the SCInc and SCLAlf soils (Table 6). By contrast, aforementioned soil water availability parameters (PAW, LLWR, and IWC) significantly increased with increasing biochar application rate in the LArid soil (Table 6). There were no significant differences between soils treated by BC300 or BC600. LLWR decreased by 32 to 44% in the SCInc and SCLAlf soils while it increased by 32 to 61% in the LArid soil amended with 3BC in comparison to the control (0BC). In addition, IWC decreased by 21 to 35% in the SCInc and SCLAlf soils while it increased by 44 to 46% in the LArid soil amended with 3BC as compared to the control (Table 6). The PAW, LLWR, and IWC were lower in the LArid soil, with greater GSD in the control soils, but they reached higher values when treated with 3% biochar. It seems that soil GSD is the most important factor for changing soil water availability after biochar amendment. This finding corroborates the ideas

Soil	Biochar	Rate (%wt)	PAW (cm^3 cm^{-3})	LLWR (cm^3 cm^{-3})	IWC (cm^3 cm^{-3})	EI_{IWC} (J kg^{-1})	FC (cm^3 cm^{-3})	PWP (cm^3 cm^{-3})	h_{PR-2} (cm)	θ_{A-10} (cm^3 cm^{-3})	S (cm^{-1})	h_i (cm)
SCInc	BC300	0	0.143^{a}	0.100^{a}	0.136^{a}	32.14^{c}	0.346^{d}	0.203^{d}	2555^{d}	0.413^{d}	0.076^{ab}	92.23^{a}
		1	0.108^{b}	0.086^{b}	0.127^{b}	67.80^{b}	0.388^{c}	0.279^{c}	3692^{c}	0.444^{c}	0.077^{a}	54.14^{b}
		2	0.081^{c}	0.076^{c}	0.120^{c}	112.63^{a}	0.409^{b}	0.328^{b}	8217^{b}	0.472^{b}	0.072^{b}	42.38^{b}
		3	0.056^{c}	0.056^{d}	0.107^{d}	112.67^{a}	0.424^{a}	0.368^{a}	16733^{a}	0.499^{a}	0.077^{a}	34.79^{b}
	BC600	0	0.143^{a}	0.100^{a}	0.136^{a}	32.14^{c}	0.346^{c}	0.203d	2555^{c}	0.413^{b}	0.076^{a}	92.23^{a}
		1	0.116^{b}	0.092^{b}	0.107^{b}	94.44^{b}	0.429^{b}	0.313^{c}	4191^{b}	0.445^{ab}	0.067^{b}	62.43^{b}
		2	0.081^{c}	0.071^{c}	0.090^{c}	111.00^{ab}	0.458^{a}	0.376^{b}	5517^{a}	0.476^{a}	0.065^{b}	50.07^{c}
		3	0.057^{d}	0.057^{d}	0.088^{c}	140.82^{a}	0.462^{a}	0.406^{a}	4985^{a}	0.474^{a}	0.067^{b}	38.73^{c}
SCLAlf	BC300	0	0.113^{a}	0.095^{a}	0.157^{a}	73.40^{c}	0.299^{d}	0.186^{d}	4544^{c}	0.398^{c}	0.079^{b}	67.51^{a}
		1	0.089^{b}	0.078^{b}	0.126^{b}	74.21^{c}	0.363^{c}	0.278^{c}	4698^{c}	0.425^{bc}	0.086^{a}	53.14^{ab}
		2	0.071^{bc}	0.068^{c}	0.112^{c}	159.91^{a}	0.395^{b}	0.324^{b}	9607^{b}	0.456^{ab}	0.078^{b}	45.02^{b}
		3	0.063^{c}	0.063^{d}	0.084^{d}	111.76^{b}	0.460^{a}	0.397^{a}	14619^{a}	0.476^{a}	0.064^{c}	43.21^{b}
	BC600	0	0.113^{a}	0.095^{a}	0.157^{a}	73.4^{c}	0.299^{c}	0.186^{c}	4544^{c}	0.398^{c}	0.079^{a}	67.51^{a}
		1	0.104^{a}	0.062^{b}	0.104^{b}	114.82^{b}	0.439^{b}	0.335^{b}	4793^{c}	0.426^{bc}	0.063^{c}	61.99^{a}
		2	0.065^{b}	0.063^{b}	0.092^{b}	130.82^{b}	0.436^{b}	0.371^{b}	10220^{b}	0.465^{ab}	0.070^{b}	49.59^{b}
		3	0.065^{b}	0.065^{b}	0.088^{b}	157.83^{a}	0.489^{a}	0.424^{a}	20324^{a}	0.489^{a}	0.070^{b}	46.52^{b}
LArid	BC300	0	0.090^{b}	0.079^{c}	0.107^{a}	62.12^{c}	0.154^{c}	0.064^{b}	6014^{c}	0.368^{c}	0.083^{a}	18.21^{b}
		1	0.086^{b}	0.077^{c}	0.133^{b}	100.38^{b}	0.309^{b}	0.216^{a}	6822^{c}	0.391^{c}	0.070^{b}	32.99^{b}
		2	0.133^{a}	0.125^{a}	0.175^{a}	181.28^{a}	0.349^{a}	0.223^{a}	10473^{b}	0.429^{b}	0.060^{c}	62.71^{a}
		3	0.104^{b}	0.104^{b}	0.194^{a}	158.58^{a}	0.326^{ab}	0.222^{a}	16738^{a}	0.476^{a}	0.051^{d}	73.18^{a}
	BC600	0	0.090^{b}	0.079^{b}	0.107^{a}	62.12^{c}	0.154^{b}	0.064^{b}	6014^{b}	0.368^{c}	0.083^{a}	18.21^{d}
		1	0.133^{a}	0.115^{a}	0.152^{b}	131.13^{b}	0.336^{a}	0.182^{a}	6374^{b}	0.391^{c}	0.069^{b}	62.13^{c}
		2	0.139^{a}	0.126^{a}	0.199^{a}	154.56^{ab}	0.321^{a}	0.203^{a}	8838^{b}	0.434^{b}	0.052^{c}	92.42^{b}
		3	0.127^{a}	0.127^{a}	0.226^{a}	167.07^{a}	0.332^{a}	0.205^{a}	19594^{a}	0.489^{a}	0.059^{bc}	97.60^{a}

Table 6. Mean comparisons of plant available water (PAW), least limiting water range (LLWR), integral water capacity (IWC), integral energy calculated for IWC (EI_{IWC}), field capacity (FC); permanent wilting point (PWP), matric suction at which soil penetration resistance reaches the critical value of 2 MPa (h_{PR-2}), water content at an air-filled porosity of 10% (θ_{A-10}), Dexter's index of soil physical quality (S), and matric suction at the inflection point of semi-logarithmic water retention curve (h_i) for three different soil types amended with two sugarcane bagasse-derived biochars produced at 300 °C and 600 °C and four biochar application rates. For each attribute, means correspond to various levels of each applied biochar (in each column) followed by the same lowercase letters are not significantly different ($p < 0.05$) based on the LSD test.

of Oguntunde et al.[77], who considered soil texture the most important factor in changing plant-available water after biochar amendment. On the contrary, Herath et al.[28] amended Alfisols and Andisols with the same textural class (silty loam). They reported only a significant increase in plant-available water of the Alfisols likely owing to the difference in mineral composition of the studied soils. The incorporation of 1–3% biochar significantly increased both FC by 18–116% and PWP by 79–247% in the studied soils, respectively. The more intense increment of PWP or θ_{PR-2} than FC in the SCInc or SCLAlf soils amended with the applied biochars is likely because of an increase in water retention in intra pores within biochar, leading to a reduction in the parameters of soil water availability. Bordoloi et al.[31] also stated that intra-pores of water hyacinth-derived biochar play an important role in increasing the water retention of soils. In the present study, a reverse pattern was observed in LArid soil due to the infilling effect, which led to an increase in available water. It could be reasonably argued that biochar application to coarser GSD soils (e.g., Larid soil) increased the proportion of narrow macro and meso pores, and finer pores due to the infilling effect, with the sacrifice of the wide and coarser pores[25]. Critical limits of PAW and LLWR are considered to have a cut-off form, but, in the IWC approach, these are regarded as a continuous function[47,52,53]. The upper limit of LLWR for all the samples was FC. This means that the limitation of soil aeration is removed before leaving the gravitational water. Therefore, there is good soil aeration likely resulting from improvement in structural stability. Improvement in soil structural stability resulting from biochar application leads to the appearance and distribution of soil coarse pores, thereby increasing aeration, water flow, and solute transport in the soil vadose zone. The lower limit for 55 samples was θ_{PR-2} and for 17 samples was PWP (data not shown). Therefore, it can be concluded that the high soil mechanical resistance (penetration resistance) was the main restricting factor for the water uptake by plant root at the dry end. Amending soil with biochar increased the matric suction at which soil penetration resistance reached the critical value of 2 MPa (h_{PR-2}). Amending SCInc soil with 0 to 3BC300 increased h_{PR-2} from 2555 to 16,744 cm. Therefore, biochar amendment can eliminate the restriction of high soil mechanical resistance to water uptake by plants. This can be due to the following reasons: (1) Biochar particles are highly porous medium with any pore size class especially small structural pore radii and therefore large SSA. It was reported that the porosity of biochar particles is between 70 and 90%[4]. This creates a porous environment, which resembles a semi-

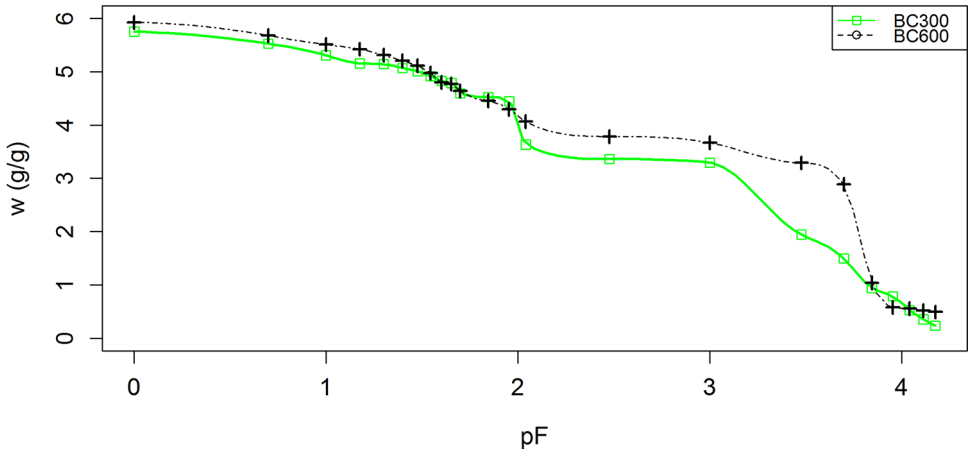

Fig. 2. Biochar water retention curves (BWRC) produced at different pyrolysis temperatures of 300 °C and 600 °C (BC300 and BC600) according to Moradi-Choghamarani et al[41].

permeable membrane and enhances retention capacity. (2) The fine-grained biochar particles with low density fill large macropores and reduce inter-pore spaces resulting in the retention of the water content that will discharge at low pressures. The tendency of biochar-treated soils to retain more water than control soil at the same water suction naturally reduces the inter-particle friction resistance. (3) Biochar particles can swell when wet to increase macro- and mesoporosity and likely its dynamic rigidity leading to a reduction in penetration resistance[40,41,78]. (4) As mentioned by Ajayi and Horn[79], weaker properties of biochar particles especially when dominant in the soil can create less resisting fabric.

Contrary to expectations, this study did not find any improvement in specific energy (integral energy) that is needed for water uptake by plants even in biochar-treated LArid soil where PAW, LLWR, and IWC increased with increasing biochar doses. Biochar amendment increased EI_{IWC} (Table 6), thereby increasing the gradient of water potential in the soil-root interface that plants must apply to absorb the available water. The increase coincided with the amount of added biochar. It would be better to say that when most of the available water is held in high h values then, EI will be high[53]. This value of high EI is under the small pore size distribution, high surface area, and surface properties of biochar particles. In terms of water absorption by plants, it seems that the water adsorbed on the surfaces of biochar particles can be divided into two categories: (1) the high-energy water that is adsorbed on the low-energy places, that is more prevalent in low-temperature biochars, where the attraction between the molecules of the solid and liquid interface is weak. Most of this water is held in low h values and is rapidly drainable due to gravity. (2) the low-energy water that is adsorbed on the high-energy places where the attraction between the molecules of the solid and liquid interface is strong. In other words, when water molecules come into contact with a solid surface, they can adsorb to it through various intermolecular forces, such as hydrogen bonding and van der Waals forces. The energy state of these adsorbed water molecules is typically lower than that of the free bulk water due to the strong interactions with the solid surface. Whereas, high-energy sites on a solid surface are areas where the surface atoms have unsatisfied bonds or are otherwise reactive. These sites can attract water molecules more strongly and form a tightly bound layer of water compared to the bulk phase water. The presence of low-energy water can influence the physical and chemical properties of the solid e.g., wetting behavior, corrosion, and catalytic activity[80,81].

High-temperature biochars due to great quantities of internal surfaces, the surface of all pore walls, are richer in such places. This liquid-like water film is strongly adsorbed and its discharge occurs in high h values. However, plants take most of their water needs from intermediate energy surfaces. The findings of the current study are better confirmed when the pure biochar (not a soil-biochar mixture) water retention curves are examined (Fig. 2). Biochar water retention curves (BWRC) were steeper at the beginning and end, and flatter in the middle (Fig. 2). The gravimetric water content remaining after applied h of 15,000 cm was about 24% w/w for BC300 and 50% w/w for BC600, which may correspond to the water contained in cryptopores[82] as well as water molecules that are held in place by strong chemical bonds.

PSD and S-index

The calculated S-index significantly decreased in response to biochar application (Tables 5 and 6). A regular pattern was not observed in SCInc-treated soil with BC300. The matric suction at the inflection point (h_i) values were significantly affected by biochar type, soil × biochar type, and soil × application rate interactions (Table 5). Amending both SCInc and SCLAlf soils with biochar significantly decreased the h_i values because of the creation of inter-aggregate macro pores, while the amount of h_i in LArid soil increased with increasing application rate of biochar due to the infilling effect and increasing the proportion of fine pores (Table 6). The h_i differed significantly among the studied soils amended with different biochar types, with the mean values of 51.6 cm for BC300 and 61.6 cm for BC600, indicating a reduction in the average soil pore size when treated with BC600 compared to BC300 (data not shown).

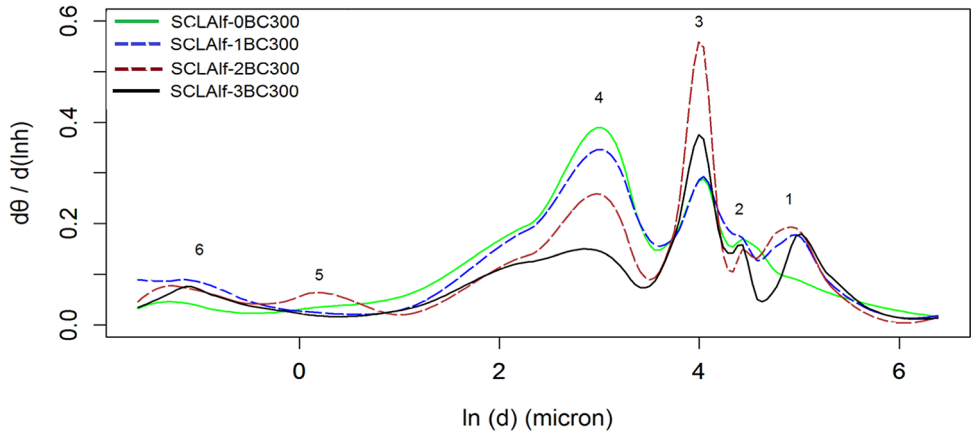

Fig. 3. Comparison between pore size distribution (PSD) of SCLAlf soil amended with 0, 1, 2, and 3% BC300.

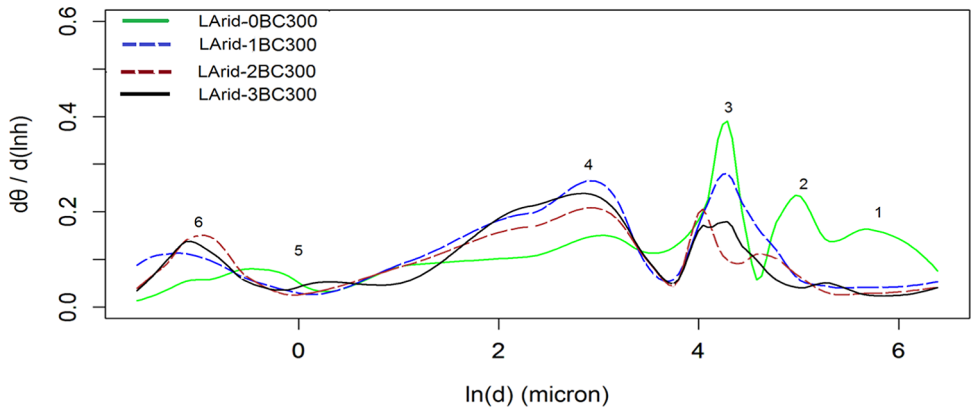

Fig. 4. Comparison between pore size distribution (PSD) of LArid soil amended with 0, 1, 2, and 3% BC600.

Figures 3 and 4 show the PSD curves for the BC300-treated SCLAlf and LArid soils derived from soil water retention data using the cubic spline function. The PSD curves in Fig. 3 exhibit six distinct peaks (numbered from 1 to 6) along the entire range of investigated pores that can also be referred to as a multimodal PSD. Many porous media do not exhibit normal or lognormal pore-size distributions. But heterogeneous multimodal distributions may be a result of the specific particle size distribution, creation of secondary porosity as a result of genetic or other processes, such as physical or chemical aggregation, biological activities, the effects of glaciation, dissolution-deposition processes which can be found in unconsolidated materials, structured soils, and fractured rocks with large pores interspersed with smaller, less permeable micropores[83]. Figures 3 and 4 represent PSD of the fine and coarse-GSD (i.e., the SCLAlf and LArid) soils treated with different rates of BC300 and BC600, respectively. In Fig. 3, the first three peaks correspond to pores with a diameter of 149, 65, and 43 µm equivalent to h of 20, 46, and 70 cm that are stronger in biochar-treated soils as compared to that of control (e.g., the first peak occurred at ln(d) = 5.004 µm, d = exp (5.004) = 149 µm, h = 2980/149 = 20 cm). These water-transmitting pores contain water molecules in inter-aggregate macro pores that rapidly drain out under gravity force. In addition, part of this water is related to the multilayer water adsorption on hydrophilic surfaces. The 4th peak in control soil is more intense than biochar-treated soils. This peak occurred at approximately h of 200 cm equivalent to the diameter of 15 µm. It may well be that the dissolution and subsequent deposition of some materials resulting from biochar caused the closure of these pores. As we mentioned in the previous section, BWR curves (Fig. 1) at h of 90 to 1000 cm (pF of 1.95 to 3) region are nearly flat. Taken together, adding biochar to the soils may have reduced the frequency of pores in this range of size. No regular pattern was observed in the 5th peak that related to h of 3000 cm. The last peak (around h of 5000 cm) represents the depletion of water molecules that are tightly bonded especially to the surface of the biochar particles and molecules that are trapped in the tiny pores. In addition to the physical restriction of water molecules in various pores, chemical interactions occur with the functional groups on the surface of the porous media. Biochar is not homogeneous in terms of morphology or site energies. Therefore, different sorption sites will have different abilities to adsorb molecules. A weaker (stronger) site may not adsorb (desorb) water before adsorption (desorption) of water onto the stronger (weaker) sites. Research during the previous decades has brought new insights into the sorption theories and the water interaction in cellulosic systems; particularly wood[84,85]. Future studies could fruitfully explore this issue on biochar. The effect of exposing wood to high temperatures, especially at temperatures above 100 °C, is

to reduce permanently the hygroscopicity (bounding water i.e. adsorption by sorption sites)[85]. In Fig. 4, the first three peaks, i.e., h of 10, 20, and 40 cm may correspond to the following two reasons: (1) the creation of large inter-aggregate porosity and multilayer adsorption of water on hydrophilic surfaces that tend to increase in peak intensity in biochar amended soils and (2) the production of fine pores due to the pore filling effect that tends to decrease in peak intensity in biochar amended soils. For coarse-textured soil, the dominance of the pore-filling effect which reduces pore throat radii, disrupts pore-connectivity and creates finer pores when soil is amended with biochar. This phenomenon is well illustrated in Fig. 5. Biochar amendment caused an increase in the 4th peak at h of 200 cm. This peak is attributed to the translocation of fine-grained biochar particles into large coarse pores which increases the fraction of medium pores (0.2 to 10 μm). The behavior of the 6th peak in the LArid soil is similar to the SCInc and SCLAlf soils. The major induced changes after biochar application occurred at h values of 0-~400 cm (on the x-axis $\ln(d) \approx 2.01$). Furthermore, it should be noted that the application of biochar due to the mentioned reasons resulted in changes in aggregation, soil stability structure, pore shape, and geometry. Consequently, changes in PSD of the biochar-treated soils have occurred.

Saffari et al.[86] stated the application of 4 w/w% corn residue biochar with particle size less than 0.5 mm into a sandy loam soil resulted in changes in the SWRC mostly at h values of 0–50 cm. Compared to the control, the application of biochar in all of the treatments caused an increase in the energy (EI) required for plants to take up a unit mass of soil water and to decrease the amount of physical quality index (except for SCInc-BC300) (Table 6).

Figure 5 schematically describes the mechanisms of fine biochar particle transportation within a soil-porous medium. In a general way, two transport mechanisms can be considered in the transport of fine biochar particles

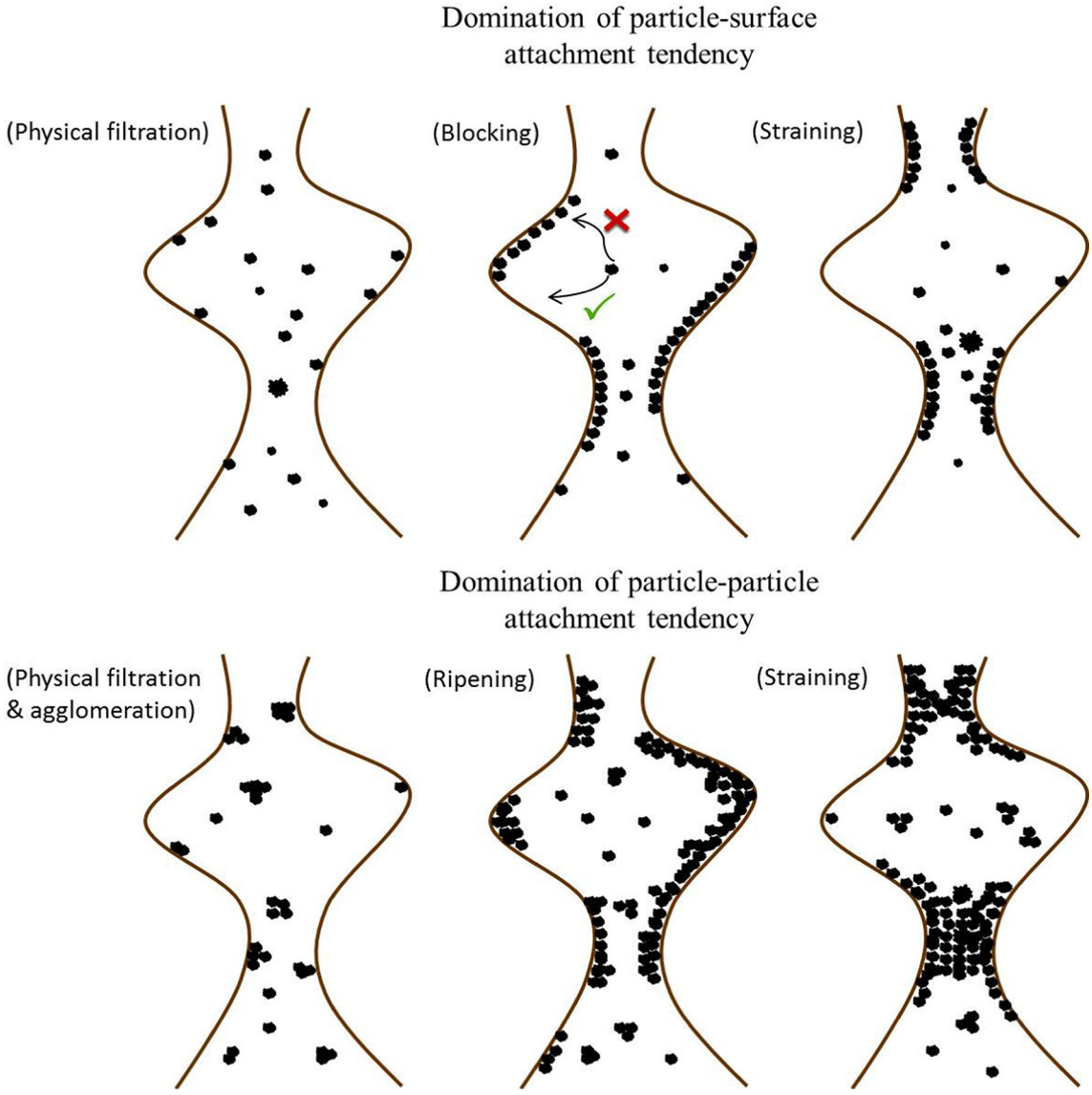

Fig. 5. Transport mechanisms in the transport of fine biochar particles in soil porous medium (adapted from Babakhani et al.[87]).

in a soil-porous medium. The first regime occurs when there is a higher particle-surface attachment affinity than the particle-particle one. In this case, the major transport mechanisms are physical filtration, site-blocking (prohibition of new particles from being adsorbed/attached on a part of a surface once capacity is filled), and physical straining or size exclusion (physical entrapment of particles in pore throats that are too small to allow particle passage or simultaneous arrival of many particles at a pore entrance). The second regime is when particle-particle attachment tendency prevails. In this mechanism, although physical filtration as well as straining may still be operative, ripening (the opposite of blocking phenomenon with an increasing trend in deposition rate over time) is predominant together with agglomeration (particle size growth that can enhance the chance of size exclusion) and further subsequent retention (Fig. 5).

Conclusion

Our research revealed that biochar significantly improves aggregation and structural stability across various soil types. Particle size distribution analysis also indicated that large inter-aggregate porosity in SCInc and SCLAlf soils increased with higher biochar rates, whereas fine pore production in LArid soil decreased. Besides, biochar-treated soils exhibited improved field capacity (FC), permanent wilting point (PWP), and effective integral water capacity (EIIWC) compared to control soils. Furthermore, the volume of drainable pores (VDP) was greater in biochar-treated SCInc and SCLAlf soils than in controls, indicating enhanced water and solute transport. Biochar mitigated high soil mechanical resistance, facilitating better water uptake by plants. However, contrary to expectations, changes in soil properties did not necessarily reduce the energy required for water uptake by plants. The study emphasizes the necessity of determining the optimum level of biochar application (3% w/w) for enhancing soil hydraulic attributes, especially in arid/semiarid regions. However, no significant differences were observed between the effects of biochar produced at 300 °C (BC300) and 600 °C (BC600). Variability among the studied soil types revealed that while LArid soil showed increased PAW, LLWR, and IWC with biochar, SCInc and SCLAlf soils experienced reductions in these parameters after treatment. In conclusion, a structural stability index (SSI) was proposed as an alternative method for evaluating aggregate stability using high energy moisture characteristic (HEMC) data. However, further exploration of integral energy (EI) and Dexter's index of soil physical quality (S) is recommended for future evaluations.

Data availability

The datasets used or analyzed during the current study are available from the corresponding author on reasonable request.

Received: 22 May 2024; Accepted: 24 October 2024
Published online: 03 November 2024

References

1. Hansen, V. et al. The effect of straw and wood gasification biochar on carbon sequestration, selected soil fertility indicators and functional groups in soil: An incubation study. *Geoderma* **269**, 99–107. https://doi.org/10.1016/j.geoderma.2016.01.033 (2016).
2. Ji, C., Cheng, K., Nayak, D. & Pan, G. Environmental and economic assessment of crop residue competitive utilization for biochar, briquette fuel and combined heat and power generation. *J. Clean. Prod.* **192**, 916–923. https://doi.org/10.1016/j.jclepro.2018.05.026 (2018).
3. Zahedifar, M., Moosavi, A. A. & Gavili, E. Monitoring soil quality indices and soybean yield as influenced by integrated biochar and drought stress. *Environ. Dev. Sustain.* https://doi.org/10.1007/s10668-023-03947-x (2023).
4. Alghamdi, A. G. Biochar as a potential soil additive for improving soil physical properties—A review. *Arab. J. Geosci.* **11**, 766. https://doi.org/10.1007/s12517-018-4056-7 (2018).
5. Paetsch, L. et al. Effect of in-situ aged and fresh biochar on soil hydraulic conditions and microbial C use under drought conditions. *Sci. Rep.* **8**, 6852. https://doi.org/10.1038/s41598-018-25039-x (2018).
6. Zama, E. F. et al. Advances in research on the use of biochar in soil for remediation: A review. *J. Soils Sediments* **18**, 2433–2450. https://doi.org/10.1007/s11368-018-2000-9 (2018).
7. Neira, J., Ortiz, M., Morales, L. & Acevedo, E. Oxygen diffusion in soils: Understanding the factors and processes needed for modeling. *Chil. J. Agric. Res.* **75**, 35–44. https://doi.org/10.4067/S0718-58392015000300005 (2015).
8. Juriga, M. & Šimanský, V. Effect of biochar on soil structure—Review. *Acta Fytotech. Zootech.* **21**, 11–19. https://doi.org/10.15414/afz.2018.21.01.11-19 (2018).
9. Hu, F. et al. Particles infiltration forces and their effects on soil aggregates breakdown. *Soil Tillage Res.* **147**, 1–9. https://doi.org/10.1016/j.still.014.11.006 (2015).
10. Šiamansky, V. & Bajcan, D. Stability of soil aggregates and their ability of carbon sequestration. *Soil Water Res.* **9**, 111–118 (2014).
11. Šiamansky, V. & Pollakova, N. Soil organic matter and sorption capacity under different soil management practices in a productive vineyard. *Arch. Agron. Soil Sci.* **59**, 1145–1154. https://doi.org/10.1080/03650340.2013.865837 (2014).
12. Jien, S. H. & Wang, C. S. Effects of biochar on soil properties and erosion potential in a highly weathered soil. *Catena* **110**, 225–233. https://doi.org/10.1016/j.catena.2013.06.021 (2013).
13. Lu, Y. et al. Biochar implications for the engineering properties of soils: A review. *Sci. Total Environ.* **888**, 164185. https://doi.org/10.1016/j.scitotenv.2023.164185 (2023).
14. Liang, B. et al. Black carbon increases cation exchange capacity in soils. *Soil Sci. Soc. Am. J.* **70**(5), 1719–1730. https://doi.org/10.2136/sssaj2005.0383 (2006).
15. Kimetu, J. M. & Lehmann, J. Stability and stabilization of biochar and green manure in soil with different organic carbon contents. *Aust. J. Soil Res.* **48**(6–7), 577–585. https://doi.org/10.1071/sr10036 (2010).
16. Khaledi, S., Delbari, M., Galavi, H., Bagheri, H. & Chari, M. M. Effects of biochar particle size, biochar application rate, and moisture content on thermal properties of an unsaturated sandy loam soil. *Soil Tillage Res.* **226**, 105579. https://doi.org/10.1016/j.still.2022.105579 (2023).
17. Rajkovich, S. et al. Corn growth and nitrogen nutrition after additions of biochars with varying properties to a temperate soil. *Biol. Fertil. Soils* **48**, 271–284. https://doi.org/10.1007/S00374-011-0624-7 (2012).
18. Bronicki, C. J. & Lal, R. Soil structure and management: A review. *Geoderma* **124**(1–2), 3–22. https://doi.org/10.1016/j.geoderma.2004.03.005 (2005).

19. Mukome, F. N. D. et al. The effects of walnut shell and wood feedstock biochar amendments on greenhouse gas emission from a fertile soil. *Geoderma* **200**(201), 90–98. https://doi.org/10.1016/j.geoderma.2013.02.004 (2013).
20. Feng, X. Chemical and mineralogical control on humic acid sorption to clay mineral surfaces. *Org. Geochem.* **36**, 1553–1566. https://doi.org/10.1016/org.geochem.2005.06.006 (2005).
21. Šiamansky, V. Effects of biochar and biochar with nitrogen on soil organic matter and soil structure in Haplic Luvisol. *Acta Fytotech. Zootech.* **19**, 129–138. https://doi.org/10.15414/afz.2016.19.04.129-138 (2016).
22. Wang, D., Fonte, S. J., Parikh, S. J., Six, J. & Scow, K. M. Biochar additions can enhance soil structure and the physical stabilization of C in aggregates. *Geoderma* **303**, 110–117. https://doi.org/10.1016/j.geoderma.2017.05.027 (2017).
23. Busscher, W. J. et al. Influence of pecan biochar on physical properties of a Norfolk loamy sand. *Soil Sci.* **175**, 10–14. https://doi.org/10.1097/SS.0b013e3181cb7f46 (2010).
24. Sun, F. & Lu, S. Biochars improve aggregate stability, water retention, and pore-space properties of clayey soil. *J. Plant Nutr. Soil Sci.* **2014**, 26–33. https://doi.org/10.1002/jpln.201200639 (2014).
25. Ajayi, A. E., Holthusen, D. & Horn, R. Changes in microstructural behavior and hydraulic functions of biochar amended soils. *Soil Tillage Res.* **155**, 166–175. https://doi.org/10.1016/j.still.2015.08.007 (2016).
26. Yang, C. D. & Lu, S. G. Effects of five different biochars on aggregation, water retention and mechanical properties of paddy soil: A field experiment of three-season crops. *Soil Tillage Res.* **205**, 104798. https://doi.org/10.1016/j.still.2020.104798 (2021).
27. Ghorbani, M. et al. Comparative effects of biochar and compost applications on water holding capacity and crop yield of rice under evaporation stress: A two-years field study. *Paddy Water Environ.* **21**(1), 47–58. https://doi.org/10.1007/s10333-022-00912-8 (2023).
28. Herath, H. M. S. K., Camps-Arbestain, M. & Hedley, M. Effect of biochar on soil physical properties in two contrasting soils: An Alfisol and an Andisol. *Geoderma* **209**(210), 188–197. https://doi.org/10.1016/j.geoderma.2013.06.016 (2013).
29. Baiamonte, G. et al. Structure alteration of a sandy-clay soil by biochar amendments. *J. Soils Sediments* **15**, 816–824. https://doi.org/10.1007/s11368-014-0960-y (2015).
30. Abbas, M. et al. Impact of biochar with different organic materials on carbon fractions, aggregate size distribution, and associated polysaccharides and soil moisture retention in an arid soil. *Arab. J. Geosci.* **12**, 626. https://doi.org/10.1007/s12517-019-4792-3 (2019).
31. Bordoloi, S. et al. Soil-biochar-water interactions: Role of biochar from *Eichhornia crassipes* in influencing crack propagation and suction in unsaturated soils. *J. Clean. Prod.* **210**, 847–859. https://doi.org/10.1016/j.jclepro.2018.11.051 (2019).
32. do Nascimento, Í. V. et al. Biochar from cashew residue enhances silicon adsorption and reduces cohesion and mechanical resistance at meso-and micro-structural scales of soil with cohesive character. *Soil Tillage Res.* **241**, 106101. https://doi.org/10.1016/j.still.2024.106101 (2024).
33. Batista, E. M. C. C. et al. Effect of surface and porosity of biochar on water holding capacity aiming indirectly at preservation of the Amazon biome. *Sci. Rep.* **8**, 10677. https://doi.org/10.1038/s41598-018-28794-z (2018).
34. Guo, H., Wai, N. C. W., Ni, J., Zhang, Q. & Wang, Y. Three-year field study on grass growth and soil hydrological properties in biochar-amended soil. *J. Rock Mech. Geotech. Eng.* **16**(7), 2764–2774. https://doi.org/10.1016/j.jrmge.2023.08.025 (2024).
35. Guo, H., Zhang, Q., Chen, Y. & Lu, H. Effects of biochar on plant growth and hydro-chemical properties of recycled concrete aggregate. *Sci. Total Environ.* **882**, 163557. https://doi.org/10.1016/j.scitotenv.2023.163557 (2023).
36. Ng, C. W. W., Guo, H., Ni, J., Qi, Z. & Chen, Z. Effects of soil-plant-biochar interactions on water retention and slope stability under various rainfall patterns. *Landslides* **19**, 1379–1390. https://doi.org/10.1007/s10346-022-01874-y (2022).
37. Ng, C. W. W. et al. Effects of plant-biochar interaction on the performance of a landfill cover system: Field monitoring and numerical modelling. *Can. Geotech. J.* **60**(11), 1663–1680. https://doi.org/10.1139/cgj-2022-0310 (2023).
38. Khormali, F. Mineralogy, micromorphology, and development of the soils in arid and semiarid regions of Fars province, Southern Iran. Ph.D. thesis. Shiraz University. Iran (2003).
39. ASTM D422-63 Standard test method for particle-size analysis of soils. https://doi.org/10.1520/D0422-63R07 (2007).
40. Moradi-Choghamarani, F., Moosavi, A. A. & Baghernejad, M. Determining organo-chemical composition of sugarcane bagasse-derived biochar as a function of pyrolysis temperature using proximate and Fourier transform infrared analyses. *J. Therm. Anal. Calorim.* **138**, 331–342. https://doi.org/10.1007/s10973-019-08186-9 (2019).
41. Moradi-Choghamarani, F., Moosavi, A. A., Sepaskhah, A. R. & Baghernejad, M. Physico-hydraulic properties of sugarcane bagasse-derived biochar: The role of pyrolysis temperature. *Cellulose* **26**, 7125–7143. https://doi.org/10.1007/s10570-019-02607-6 (2019).
42. Collis-George, N. & Figueroa, B. S. The use of soil moisture characteristics to assess soil stability. *Aust. J. Soil Res.* **22**, 349–356. https://doi.org/10.1071/SR9840349 (1984).
43. Pierson, F. B. & Mulla, D. J. An improved method for measuring aggregate stability of a weakly aggregated Loessial soil. *Soil Sci. Soc. Am. J.* **53**, 1825–1831. https://doi.org/10.2136/sssaj1989.03615995005300060057x (1989).
44. Hosseini, F., Mosaddeghi, M. R., Hajabbasi, M. A. & Sabzalian, M. R. Influence of tall fescue endophyte infection on structural stability as quantified by high energy moisture characteristic in a range of soils. *Geoderma* **249**(250), 87–99. https://doi.org/10.1016/j.geoderma.2015.03.013 (2015).
45. van Genuchten, MTh. A closed-form equation for predicting the hydraulic conductivity of unsaturated soils. *Soil Sci. Soc. Am. J.* **44**, 892–898. https://doi.org/10.2136/sssaj1980.03615995004400050002x (1980).
46. Nachabe, M. H. Macroscopic capillary length, sorptivity, and shape factor in modeling the infiltration rate. *Soil Sci. Soc. Am. J.* **60**(4), 957–962. https://doi.org/10.2136/sssaj1996.03615995006000040001x (1996).
47. de Lima, R. P., da Silva, A. R., da Silva, A. P., Leao, T. P. & Mosaddeghi, M. R. soilphysics: An R package for calculating soil water availability to plants by different soil physical indices. *Comput. Electr. Agric.* **120**, 63–71. https://doi.org/10.1016/j.compag.2015.11.003 (2016).
48. Ross, P. J., Willians, J. & Bristow, K. L. Equations for extending water retention curves to dryness. *Soil Sci. Soc. Am. J.* **55**, 923–927. https://doi.org/10.2136/sssaj1991.03615995005500040004x (1991).
49. Groenevelt, P. H., Grant, C. D. & Semetsa, S. A new procedure to determine soil water availability. *Aust. J. Soil Res.* **39**, 577–598. https://doi.org/10.1071/SR99084 (2001).
50. Mualem, Y. A new model for predicting the hydraulic conductivity of unsaturated porous media. *Water Resour. Res.* **12**, 513–522. https://doi.org/10.1029/WR012i003p00513 (1976).
51. Minasny, B. & McBratney, A. B. Integral energy as a measure of soil-water availability. *Plant Soil* **249**, 253–262. https://doi.org/10.1023/A:1022825732324 (2003).
52. Asgarzadeh, H., Mosaddeghi, M. R., Mahboubi, A. A., Nosrati, A. & Dexter, A. R. Soil water availability for plants as quantified by conventional available water, least limiting water range and integral water capacity. *Plant Soil* **335**, 229–244. https://doi.org/10.1007/s11104-010-0410-6 (2010).
53. Asgarzadeh, H., Mosaddeghi, M. R., Mahboubi, A. A., Nosrati, A. & Dexter, A. R. Integral energy of conventional available water, least limiting water range and integral water capacity for better characterization of water availability and soil physical quality. *Geoderma* **166**, 34–42. https://doi.org/10.1016/j.geoderma.2011.06.009 (2011).
54. Satyanaga, A., Rahardjo, H., Leong, E. C. & Wang, J. Y. Water characteristic curve of soil with bimodal grain-size distribution. *Comput. Geotech.* **48**, 51–61. https://doi.org/10.1016/j.compgeo.2012.09.008 (2013).
55. Kutilek, M. & Nielsen, D. R. *Soil Hydrology*, 370. https://journals.lww.com/soilsci/Fulltext/1996/02000/Soil_Hydrology_.9.aspx (Catena Verlag, Germany, 1994).

56. Kastanek, F. J. & Nielsen, D. R. Description of soil water characteristics using cubic spline interpolation. *Soil Sci. Soc. Am. J.* **65**, 279–283. https://doi.org/10.2136/sssaj2001.652279x (2001).
57. Cassaro, F. A. M., Borkowski, A. K., Pires, L. F., Rosa, J. A. & Saab, S. D. C. Characterization of a Brazilian clayey soil submitted to conventional and no-tillage management practices using pore size distribution analysis. *Soil Tillage Res.* **111**, 175–179. https://doi.org/10.1016/j.still.2010.10.004 (2011).
58. Dexter, A. R. Soil physical quality. Part I. Theory, effects of soil texture, density, and organic matter, and effects on root growth. Unsaturated hydraulic conductivity and general conclusions about S-theory. *Geoderma* **120**, 201–214. https://doi.org/10.1016/j.geoderma.2003.09.004 (2004).
59. USDA. Soil survey manual. In: *Soil Survey Division Staff; Soil Conservation Service Volume Handbook 18 (chapter 3)* (U.S. Department of Agriculture, 2017).
60. Bonelli, P. R., Buonomo, E. L. & Cukierman, A. L. Pyrolysis of sugarcane bagasse and co-pyrolysis with an Argentinean subbituminous coal. *Energy Sources Part A* **29**, 731–740. https://doi.org/10.1080/00908310500281247 (2007).
61. Tomczyk, A., Sokołowska, Z. & Boguta, P. Biochar physicochemical properties: Pyrolysis temperature and feedstock kind effects. *Rev. Environ. Sci. Biotechnol.* **19**, 191–215. https://doi.org/10.1007/s11157-020-09523-3 (2020).
62. Ghorbani, M. et al. How do different feedstocks and pyrolysis conditions effectively change biochar modification scenarios? A critical analysis of engineered biochars under H_2O_2 oxidation. *Energy Convers. Manag.* **300**, 117924. https://doi.org/10.1016/j.enconman.2023.117924 (2024).
63. Katyal, S., Thambimuthu, K. & Valix, M. Carbonisation of bagasse in a fixed bed reactor: Influence of process variables on char yield and characteristics. *Renew Energy* **28**, 713–725. https://doi.org/10.1016/S0960-1481(02)00112-X (2003).
64. Chen, B. & Chen, Z. Sorption of naphthalene and 1-naphthol by biochars of orange peels with different pyrolytic temperatures. *Chemosphere* **76**, 127–133. https://doi.org/10.1016/j.chemosphere.2009.02.004 (2009).
65. Rafiq, M. K. et al. Influence of pyrolysis temperature on physicochemical properties of corn stover (*Zea mays* L.) biochar and feasibility for carbon capture and energy balance. *PLoS ONE* **11**, e0156894. https://doi.org/10.1371/journal.pone.0156894 (2016).
66. Li, X. et al. Functional groups determine biochar properties (pH and EC) as studied by two-dimensional ^{13}C NMR correlation spectroscopy. *PLoS ONE* **8**(6), e65949. https://doi.org/10.1371/journal.pone.0065949 (2013).
67. Zhao, S. X., Na, T. & Wang, X. D. Effect of temperature on the structural and physicochemical properties of biochar with apple tree branches as feedstock material. *Energies* **10**, 1293. https://doi.org/10.3390/en10091293 (2017).
68. Li, J. et al. Comparative study for microcystin-LR sorption onto biochars produced from various plant- and animal-wastes at different pyrolysis temperatures: Influencing mechanisms of biochar properties. *Bioresour. Techol.* **247**, 794–803. https://doi.org/10.1016/j.biortech.2017.09.120 (2018).
69. Suliman, W. et al. The role of biochar porosity and surface functionality in augmenting hydrologic properties of a sandy soil. *Sci. Total Environ.* **574**, 139–147. https://doi.org/10.1016/j.scitotenv.2016.09.025 (2017).
70. Downie, A., Crosky, A. & Munroe, P. Physical properties of biochar. In *Biochar for Environmental Management—Science and Technology* (eds Lehmann, J. & Joseph, S.) 227–249 (Earthscan, 2009). https://doi.org/10.4324/9781849770552.
71. Zhao, Z. & Zhou, W. Insight into interaction between biochar and soil minerals in changing biochar properties and adsorption capacities for sulfamethoxazole. *Environ. Pollut.* **245**, 208–217. https://doi.org/10.1016/j.envpol.2018.11.013 (2019).
72. Hardie, M., Clothier, B., Bound, S., Oliver, G. & Close, D. Does biochar influence soil physical properties and soil water availability?. *Plant Soil* **376**, 347–361. https://doi.org/10.1007/s11104-013-1980-x (2014).
73. Ojeda, G. et al. Are soil–water functions affected by biochar application?. *Geoderma* **249–250**, 1–11. https://doi.org/10.1016/j.geoderma.2015.02.014 (2015).
74. Eastman, C. M. Soil physical characteristics of an Aeric Ochraqualf amended with Biochar. Graduate Program in Environmental and Natural Resources. The Ohio State University, Columbus. https://etd.ohiolink.edu (2011).
75. Akhtar, J., Galloway, A. F., Nikolopoulos, G., Field, K. J. & Knox, P. A quantitative method for the high throughput screening for the soil adhesion properties of plant and microbial polysaccharides and exudates. *Plant Soil* **428**, 57–65. https://doi.org/10.1007/s11104-018-3670-1 (2018).
76. Newcomb, C.J., Qafoku, N.P., Grate, J.W., Bailey, V.L., De Yoreo, J.J. Developing a molecular picture of soil organic matter–mineral interactions by quantifying organo–mineral binding. *Nature Commun.* **8**, 396. https://doi.org/10.1038/s41467-017-00407-9 (2017).
77. Oguntunde, P. G., Fosu, M., Ajayi, A. E. & Van De Giesen, N. Effects of charcoal production on maize yield, chemical properties and texture of soil. *Biol. Fertil. Soils* **39**, 295–299. https://doi.org/10.1007/s00374-003-0707-1 (2004).
78. Zong, Y., Chen, D. & Lu, S. Impact of biochars on swell–shrinkage behavior, mechanical strength, and surface cracking of clayey soil. *J. Plant Nutr. Soil Sci.* **177**(6), 920–926. https://doi.org/10.1002/jpln.201300596 (2014).
79. Ajayi, A. E. & Horn, R. Biochar-induced changes in soil resilience: Effects of soil texture and biochar dosage. *Pedosphere* **27**, 236–247. https://doi.org/10.1016/S1002-0160(17)60313-8 (2017).
80. Yuet, P. K. & Blankschtein, D. Molecular dynamics simulation study of water surfaces: Comparison of flexible water models. *J. Phys. Chem. B* **114**(43), 13786–13795 (2010).
81. Israelachvili, J. N. *Intermolecular and Surface Forces*. 3rd edn. ISBN: 9780128102947, (Elsevier, 2011).
82. Alaoui, A., Lipiec, J. & Gerke, H. H. A review of the changes in the soil pore system due to soil deformation: A hydrodynamic perspective. *Soil Tillage Res.* **115**, 1–15. https://doi.org/10.1016/j.still.2011.06.002 (2011).
83. Alfaro Soto, M. A., Lenhard, R., Chang, H. K. & van Genuchten, MTh. Determination of specific LNAPL volumes in soils having a multimodal pore-size distribution. *J. Environ. Manag.* **237**, 576–584. https://doi.org/10.1016/j.jenvman.2019.02.077 (2019).
84. Hartley, I. & Hamza, M. F. Wood: Moisture content, hygroscopicity, and sorption. In *Reference Module in Materials Science and Materials Engineering* (ed. Hashmi, S.) (Elsevier, 2016). https://doi.org/10.1016/B978-0-12-803581-8.02219-0.
85. Hartley, I. D., Kamke, F. A. & Peemoeller, H. Cluster theory for water sorption in wood. *Wood Sci. Technol.* **26**, 83–99. https://doi.org/10.1007/BF00194465 (1992).
86. Saffari, N., Hajabbasi, M. A., Shirani, H., Mosaddeghi, M. R. & Owens, G. Influence of corn residue biochar on water retention and penetration resistance in a calcareous sandy loam soil. *Geoderma* **383**, 114734. https://doi.org/10.1016/j.geoderma.2020.114734 (2021).
87. Babakhani, P., Bridge, J., Doong, R. & Phenrat, T. Continuum-based models and concepts for the transport of nanoparticles in saturated porous media: A state-of-the-science review. *Adv. Coll. Interface Sci.* **246**, 75–104. https://doi.org/10.1016/j.cis.2017.06.002 (2017).

Acknowledgements

The authors acknowledge the financial support of Shiraz University.

Author contributions

F.M.C.: Investigation, methodology, modeling, writing-original draft and editing. A.A.M.: Investigation, methodology, writing-review and editing, funding acquisition, and supervision. A.R.S.: Adviser, review and editing.

Funding
This study was funded by Shiraz University.

Declarations

Competing interests
The authors declare no competing interests.

Additional information
Correspondence and requests for materials should be addressed to A.A.M.

Reprints and permissions information is available at www.nature.com/reprints.

Publisher's note Springer Nature remains neutral with regard to jurisdictional claims in published maps and institutional affiliations.